Alloying of hydroxyapatite onto Ti6Al–4V by high power laser irradiation

F. LUSQUIÑOS, J. POU, J. L. ARIAS, M. BOUTINGUIZA, B. LEÓN, M. PÉREZ-AMOR
Dpto. Física Aplicada, Universidade de Vigo, Lagoas-Marcosende 9, E-36200 Vigo, Spain
F. C. M. DRIESSENS
University of Nijmegen, Calcio B.V., Ohe En Laak, Netherlands

In the biomedical field, the synthetic hydroxyapatite [$Ca_{10}(PO)_4(OH)_2$], with similarity to the inorganic component of bone but brittle, has been considered as the appropriate coating on stronger implant materials, such as metallic implants, for presenting a surface which is conductive to bone formation.

Many industrial and laboratory techniques were developed to apply hydroxyapatite onto metallic substrates, such as electrophoretic deposition, ion sputtering, hot isostatic pressing, pulsed laser deposition and the only widely used method commercially available: plasma spraying.

This work presents a new approach on how to bind calcium phosphate (CaP) to the Ti alloy with a well-known technique in the metallurgical field: laser surface alloying, in order to overcome the drawbacks of plasma spraying. The analysis of the results obtained and the description of the phenomena that take place in the coating process will complete this explorative study.

1. Introduction

Calcium phosphate ceramics, especially hydroxyapatite (HA) are currently used as biomaterials for many applications in both dentistry and orthopedics, because they form a real bond with the surrounding bone tissue when implanted [1]. Nevertheless, due to the poor mechanical properties of bulk HA ceramics, these cannot be used as implant devices to replace large bony defects for major load-bearing applications [2]. In those cases, titanium-based devices find their field of utilization. For this reason, much effort has been devoted in the last decade, towards the application of HA as a coating on metallic substrates, in order to improve fixation and promote osteointegration of cementless titanium-based implant devices [3].

The plasma-spray (PS) technique is the only widely used method commercially available for coating implant devices with HA. But the PS HA coatings, although exhibiting a very good biocompatibility, present some disadvantages affecting the long-term stability of the implant and, therefore, its lifetime. Among these drawbacks, the most significant are the poor coating-substrate adherence (making it necessary to introduce a grit-blasting surface treatment prior to the coating procedure, in order to guarantee a minimum adhesion of the coating) and the lack of uniformity of the coating from two different points of view: morphology and crystallinity [4–8].

Because of these drawbacks, several techniques have been proposed to apply HA as a coating on metallic substrates, such as electrophoretic deposition [9], magnetron sputtering deposition [10], ion-beam deposition [11] and pulsed laser deposition (PLD) [12–15]. Up to now, the PLD technique appears to be the most promising one, because it allows the intrinsic disadvantages of the PS technique to be overcome [16].

However, direct pulsed-laser irradiation of a powder being a mixture of brushite and calcite on a stainless-steel surface appeared to lead also to the formation of a ceramic coating containing apatite [17]. Such a direct laser irradiation might be used for a sort of welding or ''alloying'' of HA particles onto Ti6Al–4V alloy, which is used most frequently for load-bearing implants. The purpose of the present study was to explore the processes that take place when a substantial part of the alloy and the calcium phosphate were in the form of a melt.

2. Materials and methods

2.1. Materials

Ti alloy (Ti6Al–4V) plates with a thickness of 6 mm and dimensions of $50 \times 50\,mm^2$ were used as substrates without a special surface finishing after normal machining. The composition of the Ti6Al–4V is as follows: 0.01% C, 0.006% H, 0.18% Fe, 6.07% Al, 3.94% V and 89.79% Ti.

The hydroxyapatite powder (LAH-97) was supplied by Fin-Ceramica Faenza (Italy) having a particle size

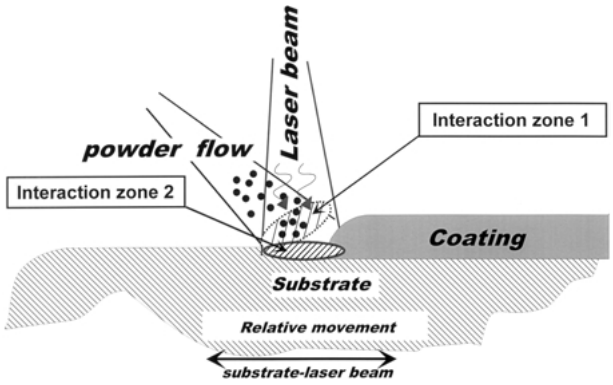

Figure 1 Schematic illustration of the laser alloying process.

distribution ranging from 50 to 500 μm showing a heterogeneous shape. The Ca : P molar ratio value of 1.68 confirms the quasi stoichiometric composition of the HA, which, at the same time, presents a high crystallinity ($\geq 95\%$) as it was demonstrated by X-ray diffraction (XRD).

2.2. Experimental system

The route selected to apply the HA powder as a coating is the laser surface alloying. A schematic drawing of this method is shown in Fig. 1. This technique consists basically in blowing particles of the precursor material by a carrier gas over the metallic substrate that is moving across this powder flow and the laser beam. A stationary high power laser radiation is directed to the surface of the substrate. The laser beam heats up the precursor material cloud and creates a molten-pool on the metallic substrate where the particles impinge. To avoid the oxidation in the interaction zone, a shielding inert gas is applied. A rapid quenching takes place when the molten-pool goes away from the laser irradiated area. Thus, the final result is a coating on the surface of the metallic substrate.

In this work a pulsed Nd : YAG laser (Rofin Sinar RSY 500 P) was used. This laser emits infrared radiation (wavelength: 1064 nm) in a way in which the pulse duration, the frequency of the pulses and the mean power are tuneable. The laser beam was coupled to a fiber optics (core diameter: 400 μm) in order to guide the energy from the laser source to the workpiece. The power density obtained over the titanium alloy substrate has exceeded 8000 W/cm^2, at a frequency of 40 Hz and 4 ms of pulse duration. The relative speed between the laser beam and the Ti6Al–4V substrate was set to 1 mm/s.

2.3. Structural and morphological examination

Coated samples were characterized using several analytical techniques, including scanning electron microscopy (SEM), energy dispersive X-ray spectroscopy (EDX) and XRD.

XRD analyses were carried out with a Siemens D-5000 diffractometer using CuKα radiation at 40 kV and 30 mA. The coatings were scanned in the standard θ to 2θ geometry from 10° to 60° with steps of 0.1° 2θ for 50 s. The resulting XRD spectra were compared with the Joint Committee of Powder Diffraction Standard (JCPDS) files.

The samples were gold coated to be examined using a Philips XL30 scanning electron microscope (SEM) with an accelerating voltage of 12 kV. The composition analysis was performed by means of an EDAX energy dispersive X-ray spectroscope.

To perform cross-sectional observations, the samples were embedded in Acryfix acrylic resin. They were then polished with a series of water-lubricated SiC papers up to grade 1000, followed by diamond paste finish up to 1 μm size. After this preparation, the samples were gold coated and examined by SEM, as in the case of the surface observation.

2.4. Interpretation of the phase compositions

The high-temperature phase diagrams [18] of the binary and ternary subsystems were used to find out which compounds and alloys might be involved in the structure of the samples. They are compiled in Table I.

3. Results and discussion

The nature of a layer obtained by means of the laser surface coating technique depends basically on the laser power density achieved on the surface of the substrate. If the target is to obtain an interfacial bond or weld without dilution of the substrate material into the coating, a moderate laser power density would be employed. In our case the process was performed with a high laser power density (8000 W/cm^2), resulting in an important degree of dilution. In this case, the coating is an alloy in which both precursor and substrate materials take part in its composition.

Fig. 2 shows the cross section of a coating-obtained by the laser surface alloying technique. As can be seen in this scanning electron micrograph, there is a certain degree of dilution of the precursor material into the substrate and the substrate itself into the coating. Observing the cross-section at higher magnification up to six different zones (labeled a–f in Fig. 3) can be distinguished. Figs 4 to 8 show scanning electron micrographs of these six zones taken at higher magnification. On the basis of the experimental XRD and EDX analysis and with the help of the knowledge

TABLE I Compilation of the phases that occur in the basic systems according to phase diagrams for ceramists

Basic systems	High-temperature phases
$CaO–P_2O_5–H_2O$	CaO, $Ca_4(PO_4)_2O$, $Ca_{10}(PO_4)_6(OH)_2$, α-$Ca_3(PO)_4$, α'-$Ca_3(PO_4)_2$, β-$Ca_3(PO_4)_2$, α-$Ca_2P_2O_7$, β-$Ca_2P_2O_7$, $Ca(PO_3)_2$, $P_2O_5[Ca_2P_6O_{17}][CaP_4O_{11}]$
$CaO–TiO_2$	CaO, $Ca_3Ti_2O_7$, $CaTiO_3$, TiO_2, $Ca_4Ti_3O_{10}$, $Ca_5Ti_4O_3$
$CaO–Al_2O_3$	CaO–$CaAl_2O_4$, $Ca_3Al_2O_6$, $CaAl_4O_7$, $CaAl_{12}O_{15}$, $Ca_{12}Al_{14}O_{33}$
$CaO–V_2O_5$	$Ca(VO_3)_2$, $Ca_2V_2O_7$, $Ca_3(VO_4)_2$
$Al_2O_3–TiO_2$	Al_2TiO_5 (α and β)
$Al_2O_3–P_2O_5$	$AlPO_4$, $Al(PO_3)$, Al_3PO_7
$Al_2O_3–V_2O_5$	$AlVO_4$

about the high-temperature phases compiled in Table I, all the phases present in the samples could be identified.

The surface of the coating exhibits the presence of some particles which correspond to a vanadium and phosphorous compound (point 2 in Fig. 4) into a $CaTiO_3$ matrix (point 1 in Fig. 4).

Under the surface of the coating (zone b in Fig. 3), it is possible to distinguish four different phases: the $CaTiO_3$ matrix (point 1 in Fig. 5), TiP (point 2 in Fig. 5) and VP (point 3 in Fig. 5) as aggregates and a dispersion of P (point 4 in Fig. 5) into the $CaTiO_3$ matrix.

Going deeper through the coating (zone c in Fig. 3), the phases found are only the $CaTiO_3$ matrix (point 1 in Fig. 6), the dispersion of P (point 2 in Fig. 6) into the $CaTiO_3$ matrix and Al_3PO_7 segregates (point 3 in Fig. 6).

In the region of the coating near the interface (zone d in Fig. 3) a Ti_3P_2 phase (point 2 in Fig. 7) is spread into the $CaTiO_3$ matrix (point 1 in Fig. 7).

In the interface between the coating and the substrate (zone e in Fig. 3) the presence of the original Ti alloy (Ti6Al4V) becomes more relevant (point 3 in Fig. 8). At the same time the $CaTiO_3$ (point 2 in Fig. 8), the predominant phase in the previous regions of the coating, suffers a presence reduction in this zone. A dispersion of the Ti_3P_2 phase can be also observed.

Finally, the deeper region examined (zone f in Fig. 3) shows the presence of the Ti alloy from the substrate (Ti6Al4V) which is the prevalent component (point 2 in Fig. 9), having also other phase which corresponds to the dispersion of Ti_3P_2 in the original Ti alloy (point 1 in Fig. 9) and the complete absence of $CaTiO_3$.

The results obtained were corroborated by XRD analysis (see Fig. 10) where the presence of $CaTiO_3$ is predominant.

In the laser surface alloying process two interaction zones can be distinguished (see Fig. 1). On one hand, the interaction of the laser beam with the powder flow is driven by an absorption process (interaction zone 1). As a consequence of this process the HA particles injected in

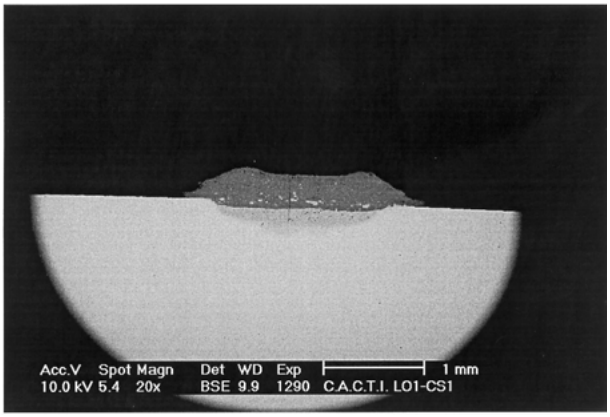

Figure 2 SEM micrograph showing the general aspect of a cross-section of the alloyed coating.

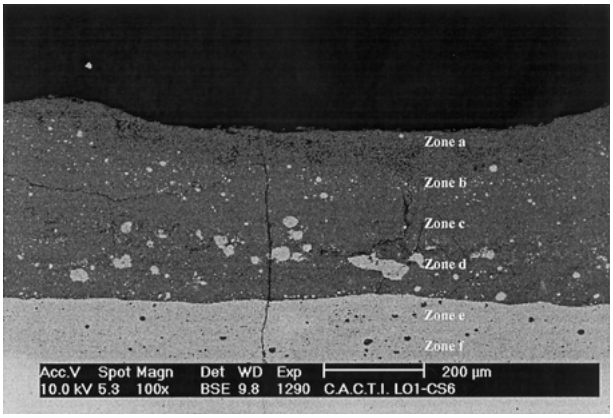

Figure 3 SEM micrograph showing the zones of interest in the alloyed coating.

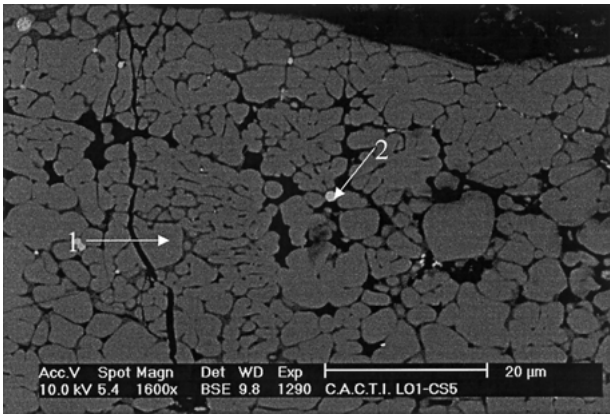

Figure 4 SEM micrograph showing the surface of the coating (zone a in Fig. 3).

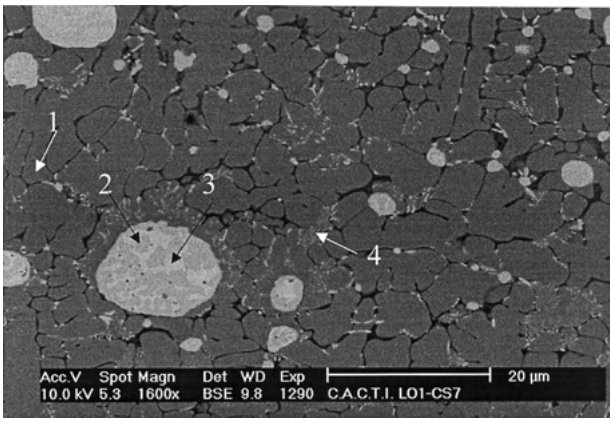

Figure 5 SEM micrograph showing the coating (zone b in Fig. 3) where the presence of $CaTiO_3$ is the predominant phase with a dispersion of V and Ti compounds.

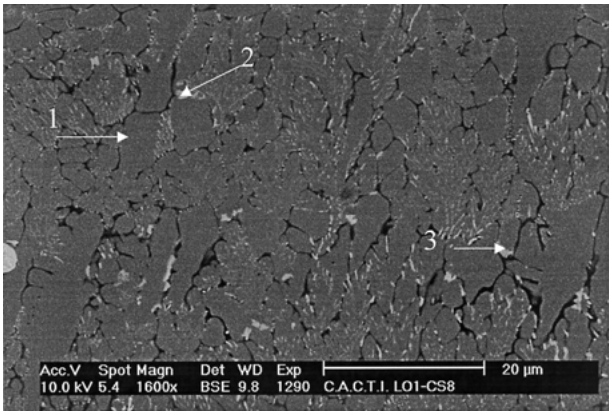

Figure 6 SEM micrograph showing the coating (zone c in Fig. 3) where it can be distinguished a dispersion of compounds of Ti and P and Ti and Al into a $CaTiO_3$ matrix.

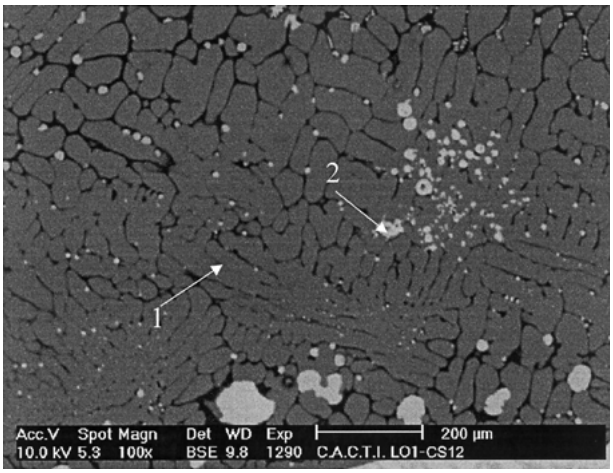

Figure 7 SEM micrograph showing the coating (zone d in Fig. 3) where a phase of Ti and P is spread into the $CaTiO_3$ matrix.

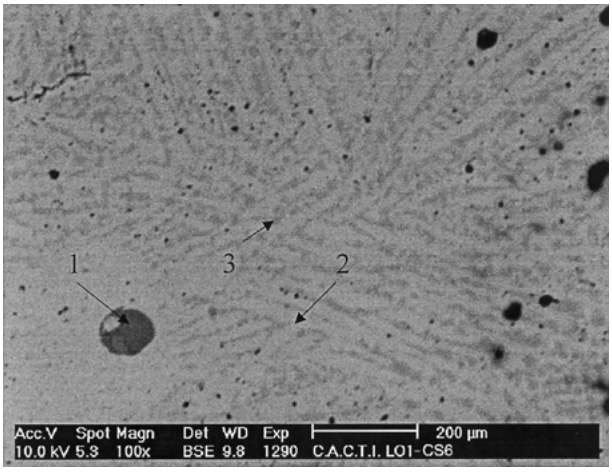

Figure 8 SEM micrograph showing the interface of the coating and the Ti alloy substrate (zone e in Fig. 3).

the form of a powder stream into this interaction zone are melted resulting in the formation of a liquid mineral. On the other hand, due to the high energy density localized in the laser spot, the surface of the Ti6Al4V melts (interaction zone 2) and forms a molten pool which is maintained in the form of liquid during the laser radiation. Thus, there are two liquids: a liquid metal

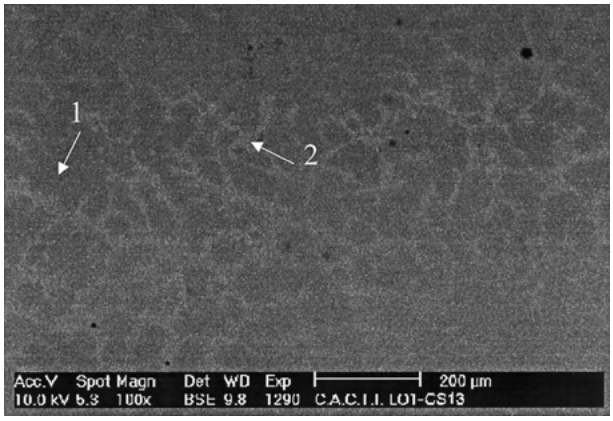

Figure 9 SEM micrograph showing the deeper zone of the interface between the coating and the Ti alloy(zone f in Fig. 3).

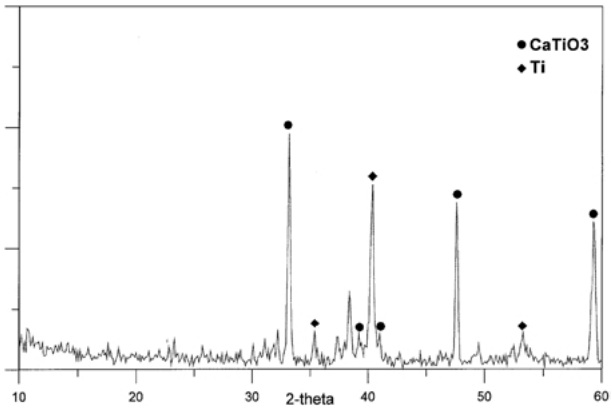

Figure 10 XRD spectrum of a laser-alloyed coating.

and a liquid mineral that due to the different bonding nature (metallic and ionic) do not show mutual solubility. Nevertheless, the flows present in the molten pool driven by superficial tension gradient and buoyancy forces promote the contact of the two liquids, taking place different reactions that can be resumed as follows:

$$2Ca_{10}(PO_4)_6O + 20Ti + 5O_2 \rightarrow 20CaTiO_3 + 12P$$

where $Ca_{10}(PO_4)_6O$ (liquid mineral) is the product of the decomposition of HA particles when the laser radiation impinges on them. The oxygen in the reaction comes from the ambient atmosphere.

XRD patterns revealed only the presence of the $CaTiO_3$ phase. This fact could be explained by the decomposition of the other calcium titanate phases via secondary reactions.

The decomposition of HA leads to the formation of water vapor. This reaction takes place in the interaction zone 1 which allows the escape of the water vapor out of the molten pool. This fact explains the absence of bubbles in the coating obtained.

The phosphorous ion is reduced to elemental phosphorous that dissolves in the metal liquid, reacting with it to form titanium phosphide, and evaporates partially. When the molten pool solidifies, the vigorous flow stops and there is a redistribution of the two liquids, in such a way that the presence of $CaTiO_3$ is dominant in the main part of the coating and the original titanium alloy, the Ti_3P_2 and the other products of the reactions

are present in the layers near the interface. Due to the fact that a rapid solidification takes place, some particles from the mineral liquid are trapped in the solidified metal and other drops from the metal liquid are trapped in the solidified mineral.

4. Conclusions

A novel technique in the biomaterials field has been explored to apply a calcium titanate layer onto the surface of a titanium alloy without the necessity of any previous treatment of the surface. This method allows applying coatings onto 3D surfaces assuring a localized and precise treatment of the pieces.

Strong fusion bonding between the calcium titanate and the titanium alloy has been achieved which can be employed as an intermediate layer to cover with a HA layer. This laser-alloyed layer will act as an anchorage for the external HA layer, thus improving the adhesion of the complete coating.

Additional work is currently in progress to study in-depth the different phenomena involved in this very complex process with the objective to explain the influence of the different processing parameters in the properties of the coating.

Acknowledgments

Technical assistance of the C.A.C.T.I. (University of Vigo) is gratefully acknowledged. This work was partially supported by the European Union through the BRITE-EURAM contract BRPR.CT97.0403, the Spanish government (CICYT MAT96-0789) and by Xunta de Galicia (Infra 94-68).

References

1. R. Z. LEGEROS, *Adv. Dent. Res.* **2** (1988) 164.
2. L. L. HENCH and J. WILSON, in ''An Introduction to Bioceramics'', edited by L. L. Hench and J. Wilson (World Scientific, Singapore, 1993) pp. 1–24.
3. J. F. KAY, *Dent. Clin. North. Amer.* **36** (1992) 1.
4. B. KOCH, J. G. C. WOLKE and K. DE GROOT, *J. Biomed. Mater. Res.* **24** (1990) 655.
5. S. R. RADIN and P. DUCHEINE, *J. Mater. Sci Mater. Med.* **3** (1992) 33.
6. M. J. FILIAGGI, R. M. PILLIAR and N. A. COOMBS, *J. Biomed. Mater. Res.* **27** (1993) 191.
7. H. JI and P. M. MARQUIS, *Biomaterials* **14** (1993) 64.
8. P. CHEANG and K. A. KHOR, *J. Mater. Proc. Technol.* **48** (1995) 429.
9. J. G. C. WOLKE, K. VAN DIJK, H. G. SCHAEKEN, K. DE GROOT and J. A. JANSEN, *J. Biomed. Mater. Res.* **28** (1994) 1477.
10. T. S. CHEN and W. R. LACEFIELD *J. Mater. Res.* **9** (1994) 1284.
11. M. SHIRKHANZADEH, M. AZADEGAN, V. STACK and S. SCHREYER, *Mater. Lett.* **18** (1994) 211.
12. C. M. COTELL, D. B. CHRISEY, K. S. GRABOWSKI, J. A. SPRAGUE and C. R. GOSSETT, *J. Appl. Biomat.* **3** (1992) 87.
13. P. BAERI, L. TORRISI, N. MARINO and G. FOTI, *Appl. Surf. Sci.* **54** (1992) 210.
14. G. SARDIN, M. VARELA and J. L. MORENZA, in ''Hydroxyapatite and Related Materials'', edited by P. W. Brown and B. Constanz (CRC Press, Boca Raton, U.S.A. 1994), p. 225.
15. E. N. ANTONOV, V. N. BAGRATASHVILI, E. N. SOBOL, R. SMITH and S. M. HOWDLE, *J. Phys. IV* (1994) C4–183.
16. F. J. GARCÍA-SANZ, M. B. MAYOR, J. L. ARIAS, J. POU, B. LEÓN and M. PÉREZ-AMOR, *J. Mater. Sci. Mater. Med.* **8** (1997) 861–865.
17. Z. YAPING, C. JIACHENG, T. JIFU and Z. ZHIRONG, *Surface and Coating Technol* **58** (1993) 125–127.
18. ''Phase diagrams for ceramists'', American Ceramic Society, 12 Volumes.

Received 1 August 2000
and accepted 23 October 2001